



3D-PRINTING-ASSISTED FABRICATION OF CHITOSAN SCAFFOLDS FROM DIFFERENT SOURCES AND CROSS-LINKERS FOR DENTAL TISSUE ENGINEERING

M. EzEldeen^{1,2,*}, J. Loos³, Z. Mousavi Nejad^{1,4}, M. Cristaldi^{1,5}, D. Murgia^{1,5}, A. Braem^{3,§} and R. Jacobs^{1,6,§}

¹OMFS IMPATH Research Group, Faculty of Medicine, Department of Imaging and Pathology, KU Leuven and Oral and Maxillofacial Surgery, University Hospitals Leuven, Kapucijnenvoer 33, 3000 Leuven, Belgium

²Department of Oral Health Sciences, KU Leuven and Paediatric Dentistry and Special Dental Care, University Hospitals Leuven, Kapucijnenvoer 33, 3000 Leuven, Belgium

³KU Leuven Department of Materials Engineering, Biomaterials and Tissue Engineering research group, Kasteelpark Arenberg 44, 3001 Leuven, Belgium

⁴Biomaterials research group, Department of Nanotechnology and Advance Materials, Materials and Energy Research Centre, P.O. box: 31787-316, Karaj, Alborz, Iran

⁵Department of Surgical, Oncological and Oral Sciences, University of Palermo, Via Liborio Giuffrè 5, 90127 Palermo, Italy

⁶Department of Dental Medicine, Karolinska Institute, Stockholm, Sweden

[§]These authors share senior authorship

Abstract

The aim of the present study was to fabricate and characterise chitosan scaffolds from animal and fungal sources, with or without gelatine as a co-polymer, and cross-linked to 3-glycidyloxypropyl trimethoxysilane (GPTMS) or genipin for application in dental root tissue engineering.

Chitosan-based scaffolds were prepared by the emulsion freeze-drying technique. Scanning electron microscopy (SEM) and nano-focus computed tomography (nano-CT) were used to characterise scaffold microstructure. Chemical composition and cross-linking were evaluated by Fourier transform infrared-attenuated total reflectance spectroscopy. Compression tests were performed to evaluate scaffold mechanical properties. Scaffold degradation was evaluated by gravimetric method and SEM. Scaffold bioactivity immersed in simulated body fluid was evaluated by SEM, with associated electron dispersive X-ray spectroscopy, and apatite formation was examined by X-ray diffraction. Finally, human dental pulp stem cells (hDPSCs) viability was evaluated.

The fabrication method used was successful in producing scaffolds with organised porosity. Chitosan source (animal *vs.* fungal), co-polymerisation with gelatine and cross-linking using GPTMS or genipin had a significant effect on scaffold properties and hDPSCs response. Chitosan-genipin (CS-GEN) scaffolds had the largest pore diameter, while the chitosan-gelatine-GPTMS (CS-GEL-GPTMS) scaffolds had the smallest. Animal chitosan-gelatine co-polymerisation increased scaffold compressive strength, while fungal chitosan scaffolds (fCS-GEL-GPTMS) had the fastest degradation rate, losing 80 % of their weight by day 21. Gelatine co-polymerisation and GPTMS cross-linking enhanced chitosan scaffolds bioactivity through the formation of an apatite layer as well as improved hDPSCs attachment and viability.

Tailored chitosan scaffolds with tuned properties and favourable hDPSCs response can be obtained for regenerative dentistry applications.

Keywords: Chitosan, fungal chitosan, dental pulp stem cells, dental tissue engineering.

***Address for correspondence:** Mostafa EzEldeen, OMFS IMPATH Research Group, Faculty of Medicine, Department of Imaging and Pathology, KU Leuven and Oral and Maxillofacial Surgery, University Hospitals Leuven, Kapucijnenvoer 33, 3000 Leuven, Belgium.
Email: mostafa.ezeldeen@kuleuven.be

Copyright policy: This article is distributed in accordance with Creative Commons Attribution Licence (<http://creativecommons.org/licenses/by-sa/4.0/>).

List of Abbreviations

ANOVA	analysis of variance
CAD	computer-aided design
CS-GEL-GPTMS	chitosan-gelatine-GPTMS
CS-GEN	chitosan-genipin
CT	computed tomography
DA	degree of acetylation
ECM	extracellular matrix
EDX	energy-dispersive X-ray analysis
FBS	foetal bovine serum
fCS-GEL-GPTMS	fungal chitosan-gelatine-GPTMS
FD	fractal dimension
FTIR-ATR	Fourier transform infrared-attenuated total reflectance spectroscopy
GPTMS	3-glycidioxypropyl trimethoxysilane
IQR	interquartile range
hDPSCs	human dental pulp stem cells
MSC	mesenchymal stem cell
MW	molecular weight
nano-CT	nano-focused CT
PBS	phosphate-buffered saline
REPs	regenerative endodontic procedures
RGD	arginine-glycine-aspartic acid
ROIs	regions of interest
SBF	simulating body fluid
SCAPs	stem cells of the apical papilla
SEM	scanning electron microscopy
SHED	stem cells from human exfoliated deciduous teeth
TERM	tissue engineering and regenerative medicine
XRD	X-ray diffraction
α MEM	Eagle's minimal essential medium alpha modification

Introduction

Oral tissues exhibit a slight regenerative capacity in response to decay, inflammation, trauma or resective surgeries. However, irreversible damage occurs frequently and a full recovery of the dentoalveolar structures is extremely challenging due to its complex anatomy (Albuquerque *et al.*, 2014; Larsson *et al.*, 2016). Recently, TERM has been explored for the replacement of injured and missing tissues, claiming promising results. Modern TERM has also opened new possibilities for regenerative dentistry. One of these is the application of REPs (Austah *et al.*, 2018; EzEldeen *et al.*, 2015; Meschi *et al.*, 2018), which aim

to repair/replace the inflamed/necrotic dentine/pulp complex to restore vascularisation, immune response, innervation and dentine deposition at a regulated rate mimicking that of the normal dentine/pulp complex (Albuquerque *et al.*, 2014; Huang and Garcia-Godoy, 2014). REPs are of particular importance in the treatment of children's immature teeth suffering pulp necrosis to induce root development and subsequent maturation (Austah *et al.*, 2018; EzEldeen *et al.*, 2015; Meschi *et al.*, 2018; Meschi *et al.*, 2019). Other more common examples are guided periodontal and alveolar bone regeneration (Larsson *et al.*, 2016). Nevertheless, current clinical protocols for dental tissue regeneration have been associated with highly variable outcomes (Larsson *et al.*, 2016; Meschi *et al.*, 2018; Meschi *et al.*, 2019). Therefore, there is a need for clinically applicable biomaterial-supported dental tissue regeneration approaches.

TERM can be approached either in a cell-free or in a cell-based manner and the choice of the appropriate scaffold plays a crucial role in both approaches. Several natural and synthetic materials have been proposed as candidates for dento-alveolar tissue engineering (Galler and D'Souza, 2011; Galler *et al.*, 2010). Chitosan has attracted much attention mainly because of its antimicrobial (Fakhri *et al.*, 2020) and immunomodulatory properties (Caires *et al.*, 2018; 2016), in addition to biocompatibility, biodegradability, low immunogenicity, gel-forming ability and osteoinductivity (Ceccarelli *et al.*, 2017; Sharma *et al.*, 2014). Chitosan is obtained by partial deacetylation of the insoluble chitin, which is a copolymer of N-acetylglucosamine and glucosamine residues linked by β -1,4-glycosidic bonds (Nwe *et al.*, 2009) as well as a natural polymer and structural element of the exoskeleton of crustaceans (such as crabs and shrimps), fungi or insects (Gathani and Raghavendra, 2016). The DA and MW of chitin can vary among members of the chitosan family (Liu *et al.*, 2016). Chitosan's drawbacks are low strength, difficulty to control pore size, possible toxicity caused by chemical modifications and inconsistent behaviour with seeded cells (Gathani and Raghavendra, 2016). Moreover, chitosan isolated from crustaceans' shells can induce a possible allergic reaction in the human body. Therefore, chitosan preparation from fungal cell walls using fermentation technologies has been suggested as an alternative for the fabrication of scaffolds used in tissue engineering (Nwe *et al.*, 2009). Fungal chitosan usually has a lower MW compared to animal chitosan, which is linked to a faster degradation rate and higher release of chitooligosaccharides (Nwe *et al.*, 2009). Chitooligosaccharides have an important role in antimicrobial activity, immunomodulation, wound healing and subsequent tissue regeneration (Batista *et al.*, 2018; Hamedi *et al.*, 2018; Nwe *et al.*, 2009). Therefore, the use of fungal chitosan might offer several advantages in the context of tissue engineering.

Chemical cross-linking agents such as glutaraldehyde and formaldehyde have been

used to enhance the stability of chitosan scaffolds. However, the risk of toxicity upon release of non-reacted groups or after degradation has led to the interest in enzymatically or naturally derived cross-linking agents (Gao *et al.*, 2014; Tonda-Turo *et al.*, 2011). GPTMS contains an epoxy and silicon alkoxide functionality and can, therefore, be used as a coupling agent (Šapić *et al.*, 2014). Genipin, found in *Gardenia jasminoides* fruit, is a natural cross-linking agent for macromolecules by binding amine groups between adjacent molecules (Gao *et al.*, 2014). Genipin has interesting properties for dental applications, as it shows anti-inflammatory properties (Mi *et al.*, 2005), and promotion of odontoblastic differentiation of human dental pulp cells (Kwon *et al.*, 2015). Further, copolymerisation of chitosan with gelatine can enhance the biological response due to the presence of the integrin-binding RGD-like sequence in gelatine that will promote cellular attachment (Kumar *et al.*, 2017).

The overall aim of the present study was to fabricate and characterise chitosan scaffolds from animal and fungal sources, with or without gelatine as a co-polymer and cross-linked to GPTMS or genipin for application in dental root tissue engineering.

Materials and Methods

Chemicals and materials

Two types of chitosan have been investigated for preparing the scaffolds: 1) chitosan of animal origin, *i.e.* 75-85 % deacetylated chitin, having a medium MW of 190-310 kDa (448877, Sigma-Aldrich); 2) fungal chitosan derived from *Aspergillus niger*, *i.e.* 70-80 % deacetylated chitin having a low MW < 30 kDa (KION. CSH.PC, KIONutrime CsG, KitoZyme s.a., Herstal, Belgium). Gelatine powder derived from porcine skin by acid-curing (type A) and having a gel strength of ~ 300 g was used as additional polymer (G2500, Sigma-Aldrich). As cross-linking agents, genipin (powder, > 98 % purity, G4796, Sigma-Aldrich; or > 98 % purity, 6902-77-8, Challenge Bioproducts, Douliu, Taiwan) and 3-glycidyloxypropyl trimethoxysilane (GPTMS, liquid, > 98 % purity, 440167, Sigma-Aldrich) were used. Acetic acid (> 99 % purity, Chem-Lab NV, Zedelgem, Belgium) was used as a solvent for chitosan. PBS was purchased from Sigma-Aldrich. SBF medium was purchased from Heraeus, Weiss Technik, Belgium. hDPSCs were cultured in α MEM (Sigma-Aldrich) supplemented with 2 mmol/L L-glutamine (Sigma-Aldrich), 100 U/mL penicillin (Sigma-Aldrich), 100 μ g/mL streptomycin (Sigma-Aldrich) and 10 % FBS (Gibco, Thermo Fisher Scientific). Serum-free MSC medium (MesenCult™-ACF Plus Medium, Stem Cell Technologies, Vancouver, Canada) was used for the metabolic activity assay. Fibronectin was purchased from Sigma-Aldrich and alamarBlue™

kit (alamarBlue™ cell viability reagent solution) from Thermo Fisher Scientific. Well plates used were 96-well plate, TPP tissue culture plates (Sigma-Aldrich) and 96-well plate, Chimney well (Fluotrac™, Greiner, Austria).

Scaffold synthesis and fabrication

Chitosan-based scaffolds were prepared by the emulsion freeze-drying technique (Fig. 1). To this end, suitable size moulds were first designed using CAD software (3-Matic, Materialise, city?, Belgium) and then 3D printed using a polyjet printer (Objet350 Connex3, Stratasys, Rehovot, Israel). Next, chitosan was dissolved in an aqueous acetic acid solution to obtain a concentration of 1.5 % (w/v), heated at 40 °C after mixing and kept under the fume hood for 3 h to remove most of the bubbles. Gelatine was added as an extra polymer to chitosan (for 2 experimental groups), with a chitosan/gelatine weight ratio of 1 : 1 (Cui *et al.*, 2014; Sakai and Kawakami, 2007). After preparing the polymer solutions, GPTMS (chitosan/GPTMS weight ratio of 1 : 1) (Chao, 2008) or genipin (animal chitosan/genipin weight ratio of 100 : 1) (Dimida *et al.*, 2017; Lluch *et al.*, 2009) were added as cross-linking agents to improve the mechanical properties and the chemical stability of the scaffolds (Sakai and Kawakami, 2007). As such, three different scaffold compositions were investigated, further referred to as chitosan-gelatine-GPTMS (CS-GEL-GPTMS), fungal chitosan-gelatine-GPTMS (fCS-GEL-GPTMS) and chitosan-genipin (CS-GEN). After solution preparation, the precursor solutions were dispensed in the moulds and immediately placed in dry ice for directional freezing to obtain radially oriented pore structure. Finally, the filled moulds were freeze-dried for 24 h and demoulded to obtain the final scaffolds (Fig. 1).

Scaffold characterisation

SEM

To visualise the internal structure of the different chitosan scaffolds, cross-sections were prepared from cylindrical freeze-dried samples by immersing them in liquid nitrogen and cutting into pieces using a razor blade. Subsequently, samples were mounted on an aluminium sample holder using double-sided carbon tape and sputter coated with a 10 nm-thick platinum layer under vacuum to achieve conductivity. Then, both cross-sections in longitudinal and transverse direction were observed by SEM (XL30 FEG, FEI Europe BV, Zaventem, Belgium). Imaging was conducted at an accelerating voltage of 5 or 10 kV, a spot size of 2 or 3, a 10 mm working distance. A low accelerating voltage and a small spot size were used to avoid charging effects. The image processing software Fiji (Image J, National Institutes of Health) (Schindelin *et al.*, 2012) was used to process the SEM images and determine the average pore size of the scaffolds by measuring the diameter of 5 pores in 5 different areas, for a total of 25 pores.

Nano-CT

To non-destructively visualise the internal pore structure in a 3D fashion, fabricated scaffolds were investigated by X-ray CT. Acquisition of CT images was carried out using a submicrometric resolution CT device (Nanotom, GE Phoenix, Blomberg, Germany). Samples were positioned on a sample holder on the rotary table ensuring that the longitudinal axis coincided with the rotary axis. Scanning was performed over 360° with a step size of 0.7°. All measurements were obtained using molybdenum target applying an operating voltage of 90 kV and a current of 250 mA during a 16.5 min exposure time for one scan. No filters were used and an isotropic voxel size of 8.5 µm could be reached. The projected radiographs were reconstructed in cross-sectional images using a commercial software package (Phoenix datosx, GE Phoenix, Wunstorf, Germany). The reconstructed nano-CT dataset was further visualised and analysed using a commercially available image analysis software (Amira, Thermo Fisher Scientific). Three ROIs (2 × 2 × 1 mm) were created from each image and were used to calculate the porosity and mean polymer strut thickness of the chitosan scaffolds.

As a measure for the 3D surface roughness of the scaffold struts, the FD was calculated from the nano-CT scans of the chitosan scaffolds. For very smooth surfaces, the FD is equal to a value of 2, while for extremely rough surfaces the FD will be approaching the limit value of 3 (Amancio *et al.*, 2020; Militký and Bajzík, 2001). Three ROIs (2 × 2 × 1 mm) were created from each image for computational reasons. ROIs were binarised to obtain 3D models for the scaffold's struts. Then, the FD was calculated for each ROI and averaged to obtain the final score for each scaffold type (Amira, Thermo Fisher Scientific).

FTIR-ATR

To investigate the chemical composition and cross-linking process, fabricated chitosan scaffolds were analysed by FTIR-ATR (Vertex 70 with platinum ATR, Bruker) Chitosan starting materials and the various cross-linking agents (genipin, GPTMS and gelatine) were analysed as controls. All samples were prepared for analysis by grinding them to a fine powder with the aid of liquid nitrogen. Spectra were taken in the range 4,000-500 cm⁻¹ at a resolution of 2 cm⁻¹ and averaged over 64 scans.

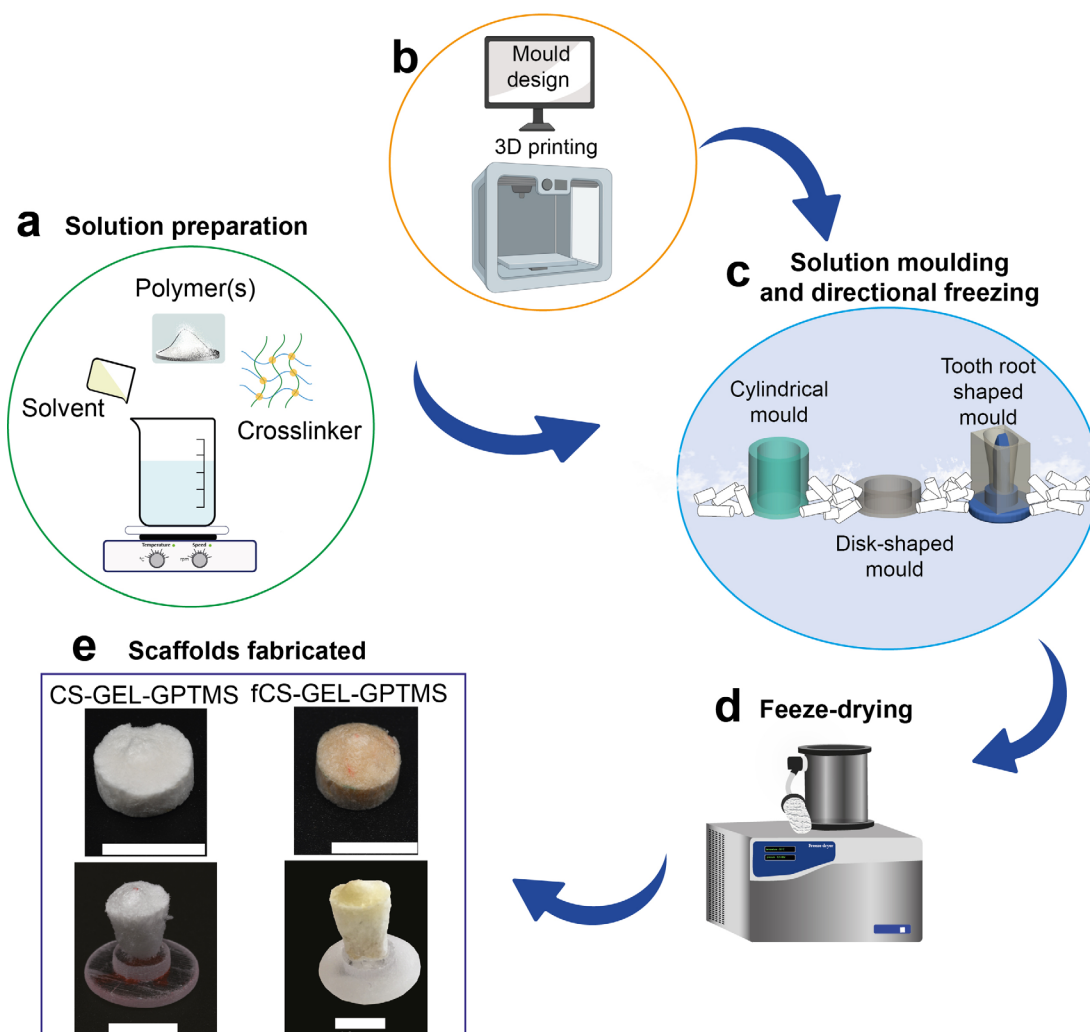


Fig. 1. Scaffold fabrication. (a) Polymer solution preparation; (b) CAD mould design and mould 3D-printing; (c) polymer moulding and directional freezing for different scaffold designs; (d) freeze-drying; (e) examples of scaffolds fabricated, scale bars: 10 mm.

Mechanical testing

To determine the load-bearing capacity of the chitosan scaffolds, compression tests were performed on cylindrical samples ($n = 5$) using a mechanical testing device (Instron 5567). A load cell of 1 kN at a crosshead speed of 1 mm/min was used. Time, load and extension were measured and captured using the Instron Bluehill software. The initial height and diameter of the samples were measured and used as input. The compressive modulus was calculated from the compressive stress-strain curve in the linear strain range, determined for each sample separately by plotting the compressive modulus in function of the strain. At least 4 samples were used to obtain reliable data.

Scaffold degradation testing

In vitro hydrolytic degradation tests were performed by incubating the scaffolds ($n = 3$ per scaffold and time point) in PBS (pH 7.4) at 37 °C under agitation for a predefined time interval. For these tests, disk-shaped (10 mm diameter and 5 mm height) samples were used in triplicate. To mimic human body conditions, a PBS buffer solution was used. This was prepared by dissolving one PBS tablet in 200 mL of deionised water at 25 °C, yielding a concentration of 0.01 mol/L phosphate buffer, 0.0027 mol/L KCl and 0.137 mol/L NaCl (pH 7.4).

After recording its initial weight, each scaffold was placed in a separate well of a 12-well cell culture plate containing 5 mL of PBS. Cell plates were placed in an incubator shaker (Innova 43, News Brunswick Scientific, Nijmegen, the Netherlands) operating at 37 °C and agitation of 60 rpm. The buffer solutions were replaced twice a week with fresh PBS. At each predetermined time interval (1, 2 or 3 weeks), scaffolds were removed from the medium, washed with distilled water to remove remaining medium and freeze-dried to ensure a constant weight. Afterwards, scaffolds were weighed again and the degradation rate was calculated using the equation:

$$\text{Degradation rate (\%)} = \frac{W_0 - W_t}{W_0} \times 100$$

where W_0 denotes the original sample weight and W_t the sample weight at the selected time point.

For each combination of scaffold type and degradation period, one replicate was examined by SEM, as described above, to compare the pore structure after varying degradation periods (1, 2 and 3 weeks) with the original pore structure.

Bioactivity testing

The scaffolds' bioactivity contributes to their potential to form an apatite layer (*i.e.* hydroxyapatite). The apatite-forming ability of all types of scaffolds was investigated by immersion in SBF, a medium with ion concentrations nearly equal to those of human blood plasma, following the technique suggested by Kokubo and Takadama (2006).

To obtain a consistent ratio of liquid to scaffold surface area, the required volume of SBF for each sample was calculated using the equation (Kokubo and Takadama, 2006):

$$V_s = S_a/10$$

where V_s is the volume of SBF (in mL) and S_a is the apparent surface area of the sample (in mm²).

For the disk-shaped samples, applying the formula resulted in a SBF volume of ~ 32 mL. For porous samples, the required volume of SBF should be larger than the calculated V_s and, therefore, a volume of 40 mL SBF for each sample was chosen. Three replicates of each type of scaffold were immersed in 40 mL SBF at 37 °C up to 3 weeks, with scaffolds being removed after 1 and 3 weeks. From day 7 onwards, the SBF was refreshed twice a week. At each selected time point, samples were removed from the SBF solution, rinsed with distilled water to remove the remaining SBF solution and dried using a vacuum desiccator (Dimida *et al.*, 2017; Kokubo and Takadama, 2006). For each combination of scaffold type and immersion time, two replicates were examined by SEM with associated EDX (EDAX, Tilburg, the Netherlands). Analysis was performed at an accelerating voltage of 15 kV, a spot size of 6 and a 11 mm working distance. Apatite formation can be recognised by a characteristic needle-like layer or by a Ca/P ratio around 1.67 (Chen *et al.*, 2015). Further, one replicate was examined by XRD (Bruker, D2 Phaser) to determine if apatite was present or not. Prior to the measurements, the chitosan scaffolds were milled using a mortar and pestle. A coupled $2\theta/\theta$ scan type (range of 5-80° in 2θ) was used, using $\text{CuK}\alpha$ ($\lambda = 0.15405$ nm) radiation as the source at a rate of 2°/min, a voltage of 40 kV and a current of 30 mA. The analysis software HighScore Plus (Malvern Panalytical, Malvern, UK) was used to identify the peaks observed in the obtained XRD spectra.

Biological evaluation

Primary cell cultures

Dental pulp tissues were acquired with informed consent from patients (15-20 years of age, male and female) undergoing extraction of third molars for therapeutic or orthodontic reasons. Written informed consent was obtained from the patients and/or their parents, as approved by the medical ethical committee of Hasselt University, Belgium (protocol 13/0104U). Pulp tissue was obtained using forceps after mechanically fracturing the extracted and disinfected tooth with surgical chisels. Pulp tissue was rinsed and kept at 37 °C in α MEM supplemented with 2 mmol/L L-glutamine, 100 U/mL penicillin, 100 μ g/mL streptomycin and 10 % FBS. hDPSCs were isolated according to the explant method and expanded in culture, as described previously (Hilken *et al.*, 2013). Cells were cultured in α MEM, enriched with 10 % heat-inactivated FBS, 2 mmol/L L-glutamine, 100 U/mL penicillin and 100 μ g/mL

streptomycin. Only mycoplasma negative cells, screened using the Plasmotest™ kit (InvivoGen), were used. All hDPSC cultures were tested by means of flow cytometry for the expression at the protein level of the following mesenchymal cell markers, as described previously (Hilkens *et al.*, 2013): positive for CD29, CD73, CD90 and CD105; negative for CD31, CD34 and CD45.

Evaluation of hDPSC viability and metabolic activity

To obtain sterile scaffolds, 24 h before seeding, scaffolds were placed in 70 % EtOH for 2 h, washed with PBS, placed in a 96-well plate and stored in an incubator until the next step. 5×10^5 cells/mL hDPSCs were seeded in 40 μ L of serum-free MSC medium on top of an uncoated scaffold ($n = 9$, per scaffold composition and time point) or a scaffold coated with

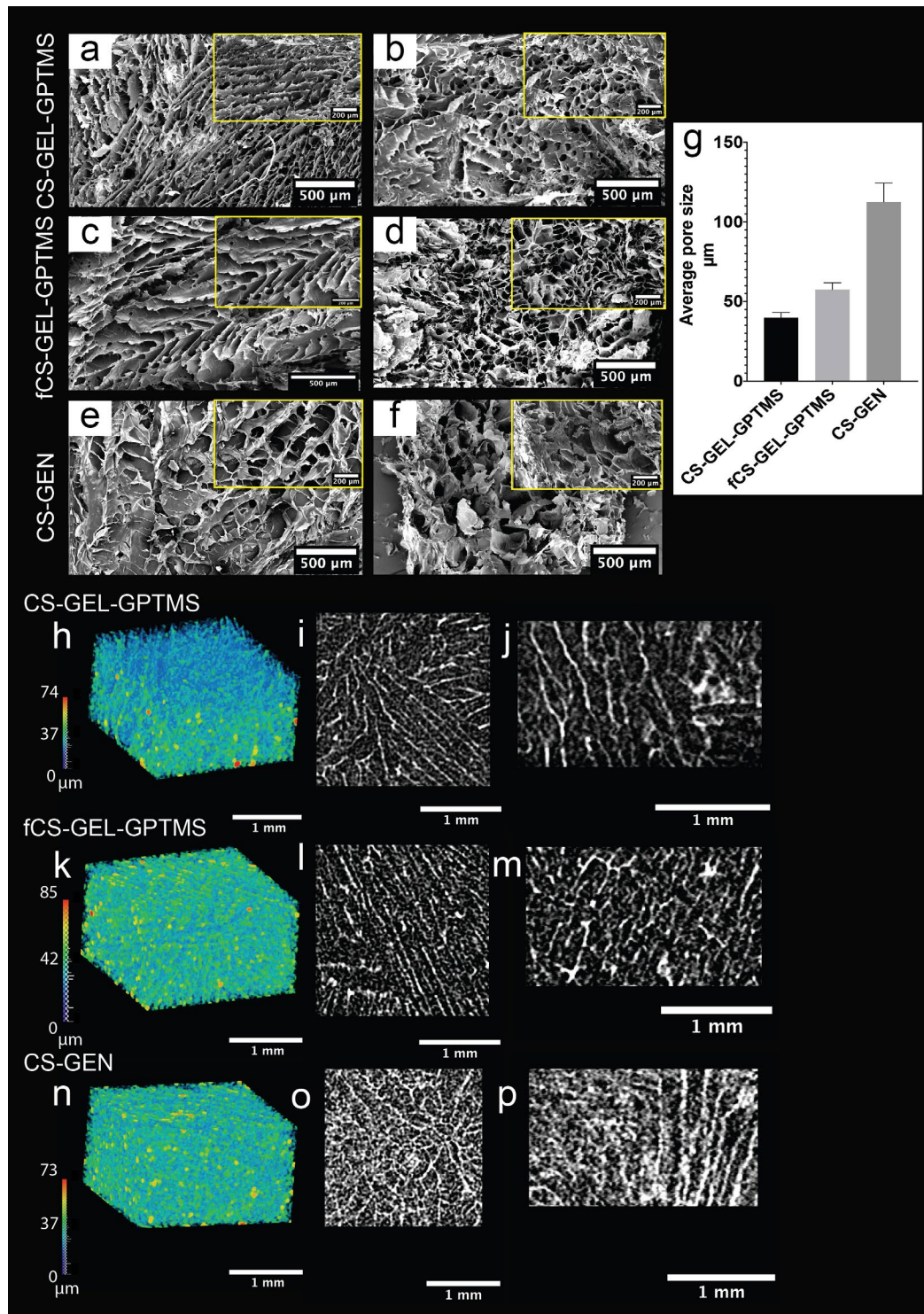


Fig. 2. Scaffolds microstructure. (a-f) Representative SEM images (higher magnification in the top right corner of each image) of (a,c,e) transverse cross-sections showing radially oriented pores and (b,d,f) longitudinal cross-sections. (g) Average pore size as measured from SEM images. (h-p) Representative nano-CT images. (h,k,n) 3D map of the strut thickness in a $2 \times 2 \times 1$ mm ROI from the different scaffolds. (i,l,o) Transverse cross-sections and (j,m,p) longitudinal cross-sections, both showing radially oriented pores.

20 $\mu\text{g}/\text{mL}$ fibronectin ($n = 9$, per scaffold composition and time point). In addition, scaffolds devoid of cells were prepared and served as blank replicates to remove background signal. Cells were allowed to attach for 30 min, then 200 μL of serum-free MSC medium supplemented with 2 mmol/L L-glutamine, 100 U/mL penicillin and 100 $\mu\text{g}/\text{mL}$ streptomycin was added to each well. 2D controls of 5×10^3 cells were seeded in a 96-well plate in two different types of culture medium: αMEM supplemented with 2 mmol/L L-glutamine, 100 U/mL penicillin, 100 $\mu\text{g}/\text{mL}$ streptomycin and 10 % FBS or serum-free MSC medium (same composition as the medium used for the scaffolds). After 1, 2, 3 and 7 d in culture, scaffolds were transferred to a new well and an alamarBlue solution (1/10 volume of the culture medium) was added to each well and incubated for 2 h at 37 °C and 5 % CO_2 . After incubation, the medium was transferred to a 96-well plate and the fluorescence excitation/emission was measured at 560/590 nm using a microplate reader (Varioskan™, Thermo Fisher Scientific). Readings of the blank replicates were subtracted to obtain the actual cell signal.

Statistical analysis

Statistical analysis was performed using GraphPad Prism for MacOS, version 9.0. (GraphPad Software). Statistical analysis (IQR method) was carried out to determine outliers and exclude them from the compressive modulus calculation. The influence of the different scaffold compositions on the compressive modulus was tested using a one-way ANOVA. The influence of the different experimental conditions and the time factor on scaffold degradation rate and cell viability was modelled using a two-way ANOVA. All ANOVA tests were followed by Tukey's correction for multiple comparisons. Statistical significance was determined at $p < 0.05$. Descriptive statistics are represented as mean \pm standard deviation.

Results

Microstructure of fabricated chitosan scaffolds

The fabrication method used was successful in producing porous scaffolds. Fig. 2 shows representative SEM cross-sectional images of the chitosan scaffolds fabricated either in the transversal (Fig. 2a,c,e) or in the longitudinal direction (Fig. 2b,d,f). It can be observed that all scaffolds exhibited a significantly different pore structure in the transverse cross-section as compared to the longitudinal cross-section. This pore anisotropy was obtained by manipulating the cooling direction during solution moulding by using dry ice only on the sides of the mould. The transverse cross-section consisted of elongated pores or radially oriented lines of pores (Fig. 2a,c,e), while these radially oriented pores were not well observed in the longitudinal cross-section. The average pore diameter of the scaffolds was determined by analysis of SEM images of the

transverse cross-sections (Fig. 2g). CS-GEN scaffolds showed the largest pore diameter of $112.6 \pm 11.8 \mu\text{m}$, followed by fCS-GEL-GPTMS scaffolds, with a pore diameter of $57.4 \pm 4.3 \mu\text{m}$. CS-GEL-GPTMS scaffolds had the smallest pore diameter of $39.8 \pm 3.2 \mu\text{m}$.

Nano-CT was used as an additional technique to evaluate the 3D pore structure of the fabricated scaffolds. Fig. 2h-p shows a 3D map of the scaffold strut thickness together with a representative transverse and longitudinal cross-section for the selected scaffolds. The radially oriented pores were observed in the transverse cross-sections of all investigated scaffolds, which matched the observations in the SEM images. Additionally, this desired pore directionality was also observed in the longitudinal cross-sections. Scaffold porosity and mean strut thickness, as calculated from the nano-CT data, revealed a comparable porosity level and mean strut thickness between all three scaffold compositions. This was 38.7 % porosity for CS-GEL-GPTMS, with a mean strut thickness of $27.1 \pm 12.2 \mu\text{m}$; 36.6 % porosity for CS-GEN, with a mean strut thickness of $26.4 \pm 11.3 \mu\text{m}$; 34.2 % porosity for fCS-GEL-GPTMS, with a mean strut thickness of $27.2 \pm 11.6 \mu\text{m}$.

Finally, the nano-CT datasets were used to calculate the FD of the scaffolds struts as a measure of 3D surface roughness. All scaffold compositions had a FD value close to 3, indicating a high surface roughness. This was 2.8 ± 0.006 for CS-GEL-GPTMS scaffolds, 2.8 ± 0.003 for fCS-GEL-GPTMS scaffolds and 2.7 ± 0.001 for CS-GEN scaffolds.

Chemical composition and cross-linking

All tested sample spectra showed absorption bands at $2,800\text{-}3,000 \text{ cm}^{-1}$ and a broad band between $3,000\text{-}3,600 \text{ cm}^{-1}$, which could be attributed to C-H stretching vibrations (symmetric and asymmetric) and an overlap of amine and alcohol stretching vibrations, respectively (Chiono *et al.*, 2008; Klein *et al.*, 2016). For the sake of simplicity, these bands are not shown and only the wave number range from $1,800$ to 650 cm^{-1} is presented.

The FTIR spectra for scaffolds obtained from animal chitosan (CS-GEL-GPTMS, Fig. 3a) and fungal chitosan (fCS-GEL-GPTMS, Fig. 3b) were similar, with approximately the same peaks, although some smaller differences could be observed. The cross-linking of GPTMS with chitosan consisted of the reaction between amine groups of the chitosan with oxirane groups in the GPTMS. This could be observed by an intensity decrease in the absorption band at $1,552 \text{ cm}^{-1}$, attributed to the N-H bending of the primary amine (Liu *et al.*, 2004). The N-H bending peak was more intense in the fCS-GEL-GPTMS spectrum, suggesting a lower degree of cross-linking (Liu *et al.*, 2004). All spectra showed bands around $1,021 \text{ cm}^{-1}$ and 920 cm^{-1} , which could be assigned to the Si-O-Si and Si-OH stretching, respectively (Connell *et al.*, 2014; Liu *et al.*, 2004; Tonda-Turo *et al.*, 2011). The presence of these bands was characteristic

for the cross-linking mechanism of GPTMS. In these spectra, bands at $1,020\text{ cm}^{-1}$ and 910 cm^{-1} were observed, associated with Si-O-Si bonds and Si-OH stretching, respectively. The presence of these bonds confirmed the successful cross-linking between chitosan and gelatine by GPTMS (Tonda-Turo *et al.*, 2011).

Fig. 3c shows the spectra for scaffolds obtained from animal chitosan crosslinked to genipin

(CS-GEN), confirming successful cross-linking as demonstrated by the presence of new peaks indicating the reaction between chitosan and genipin and the disappearance of peaks characteristic of the starting materials. The cross-linking of genipin with chitosan is a two-step process. The first, and fastest, reaction consists of the nucleophilic attack by the amino group of chitosan on the olefinic carbon atom at C3 of genipin, resulting in an opening of the

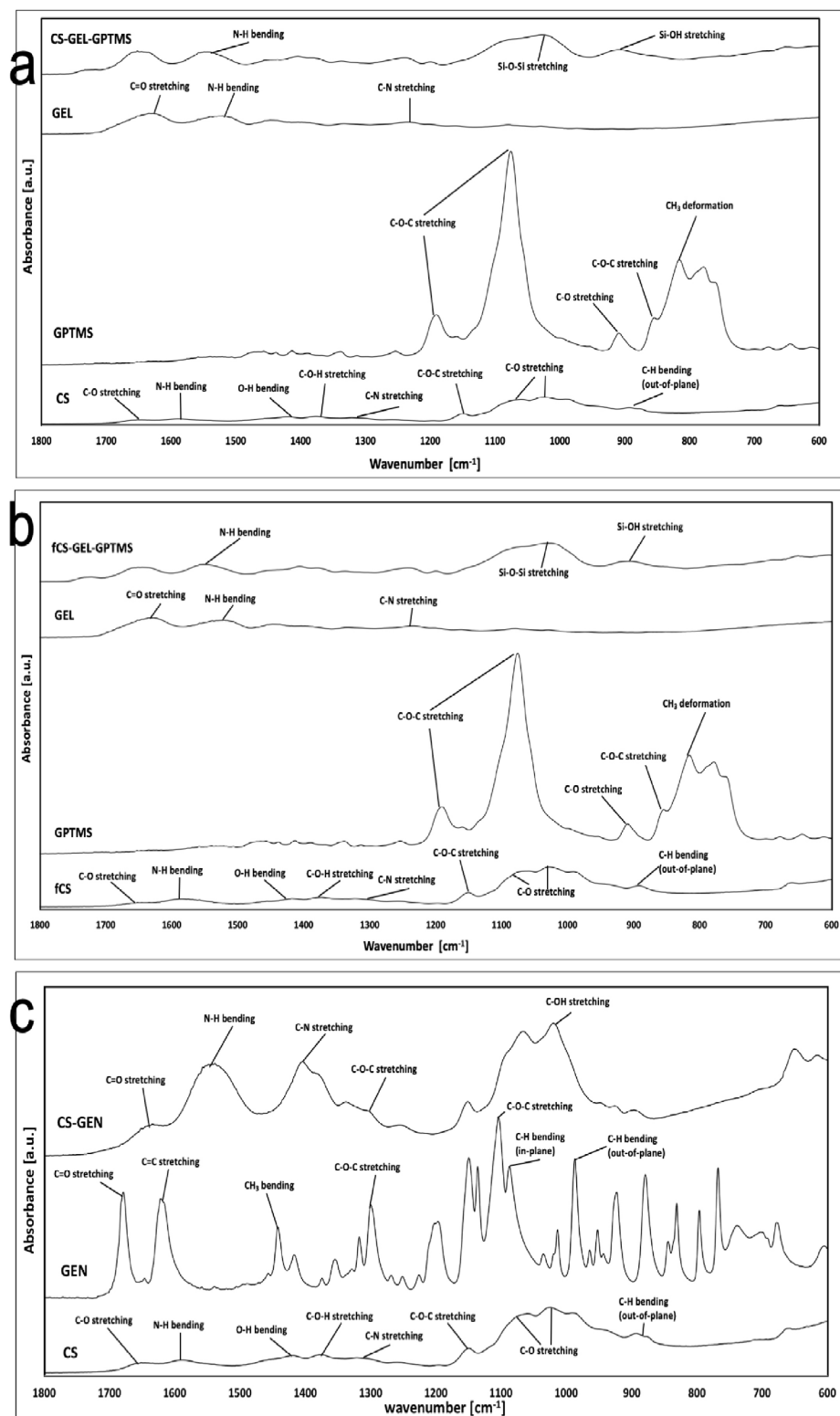


Fig. 3. Chemical composition and cross-linking. FTIR spectra of the chitosan scaffolds tested in comparison to the respective starting materials. (a) CS-GEL-GPTMS, (b) fCS-GEL-GPTMS, (c) CS-GEN.

dihydropyran ring and formation of a tertiary amine (*i.e.* a heterocyclic compound of genipin cross-linked to polymers containing primary amine groups) (Cui *et al.*, 2014; Klein *et al.*, 2016). In the FTIR spectra, this reaction can be seen by an increase in the intensity of the C-N band around $1,078\text{ cm}^{-1}$ (Cui *et al.*, 2014). The subsequent slower reaction is a nucleophilic substitution that forms an amide through the reaction of the amino group on chitosan with the ester carboxymethyl group (by C11) of genipin (Cui *et al.*, 2014; Klein *et al.*, 2016). This can be observed by the secondary amide band at $1,546\text{ cm}^{-1}$ (characteristic of

N-H bending) and the peak at $1,633\text{ cm}^{-1}$, assigned to C=O stretching in secondary amides (Klein *et al.*, 2016). Additionally, the increase in the peaks around $1,404\text{ cm}^{-1}$ and $1,015\text{ cm}^{-1}$ could be attributed to C-N stretching and C-OH stretching vibrations, respectively (Klein *et al.*, 2016).

Animal chitosan gelatine co-polymerisation increases scaffold compressive strength

CS-GEL-GPTMS scaffolds showed the highest compressive modulus ($364 \pm 30\text{ kPa}$). This was 3-fold higher than scaffolds fabricated with the fungal

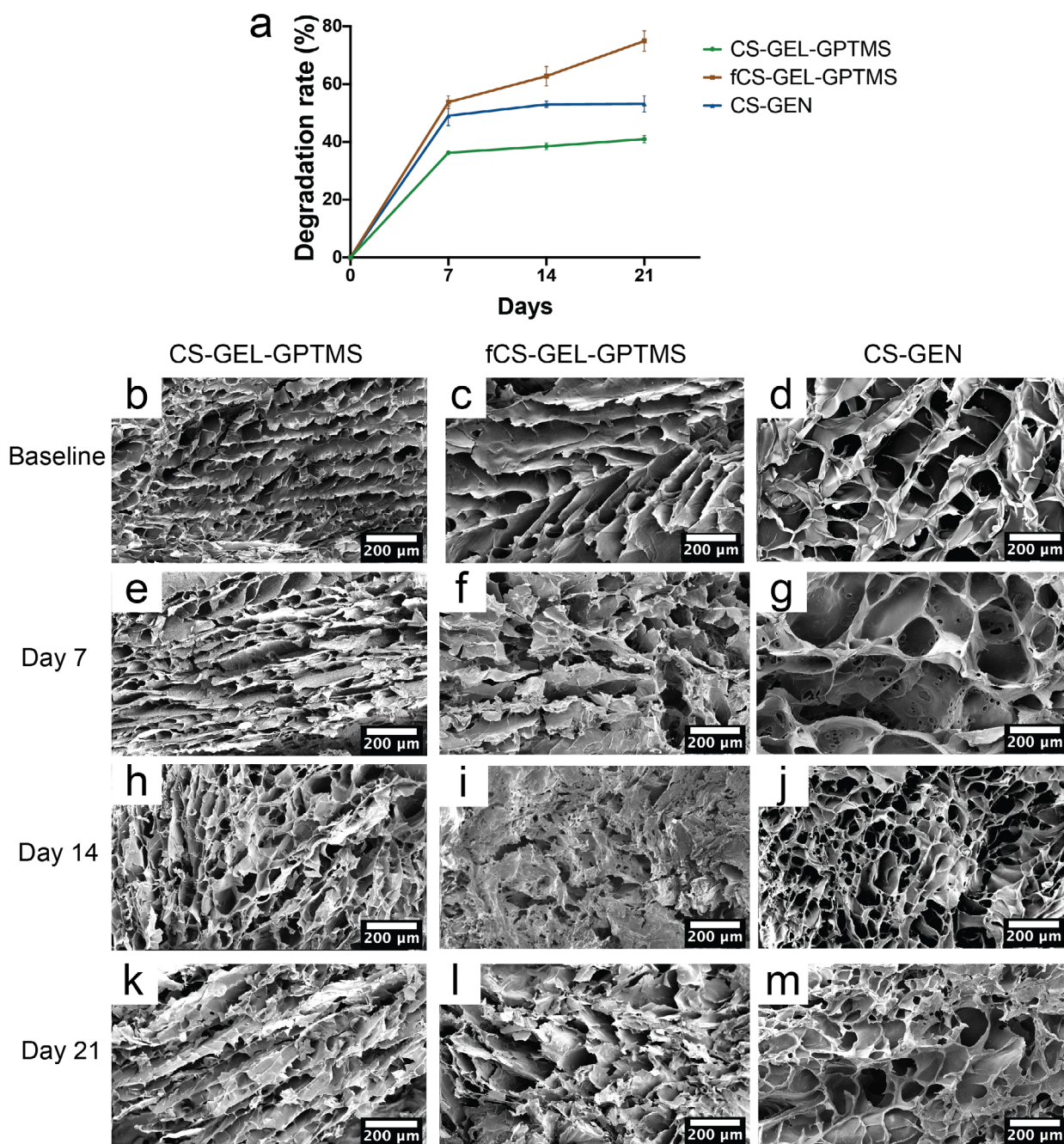


Fig. 4. Scaffolds degradation. (a) Hydrolytic degradation rate of the chitosan scaffolds showing fastest degradation rate for fCS-GEL-GPTMS scaffolds, reaching 80 % by 21 d. Data are represented as mean \pm standard deviation. (b-m) Representative SEM images of scaffold degradation up to 21 d; (f,g) fCS-GEL-GPTMS and CS-GEN scaffolds showing wider pores and rougher surfaces at 7 d; (i,l) fCS-GEL-GPTMS scaffolds showing progressive degradation leading to loss of structural organisation at 14 and 21 d matching the gravimetric results in a.

chitosan (fCS-GEL-GPTMS) (122 ± 9 kPa) and 5-fold higher than scaffolds fabricated only with animal chitosan without gelatine and crosslinked using genipin (67 ± 15 kPa).

Scaffold degradation affected by chitosan source and type of cross-linker

Scaffolds with fungal chitosan (fCS-GEL-GPTMS) showed the fastest degradation rate in PBS, followed by CS-GEN and CS-GEL-GPTMS scaffolds, respectively (Fig. 4a). There was a significant ($p < 0.05$) effect on scaffold degradation rate based on scaffold composition [F (2, 6) = 363.1, $p < 0.0001$] and time point [F (1.63, 9.79) = 1244, $p < 0.0001$]. *Post-hoc* comparisons by Tukey test showed that fCS-GEL-GPTMS scaffolds were degrading faster when compared to CS-GEL-GPTMS scaffolds at all time points ($p < 0.05$), while the difference in degradation rate was only statistically significant at day 21 compared to CS-GEN scaffolds ($p < 0.05$). The differences between CS-GEL-GPTMS and CS-GEN scaffolds were statistically significant at all time points ($p < 0.05$). For the two groups with animal chitosan, the greatest bulk of degradation occurred in the first 7 d, afterwards the degradation rate seemed to plateau up to day 21. This was in

contrast with the observations for the fungal chitosan group, where the degradation progressed steadily up to day 21 (Fig. 4a). The results from the gravimetric analysis were confirmed by the SEM images for the scaffolds at the different experimental time points (Fig. 4b-m). fCS-GEL-GPTMS scaffolds showed an increase in pore size, pore irregularity and pore surface roughness, with the porous structure changed in a sheet-like structure with bigger pores after degradation (Fig. 4c,f,i,l).

Gelatine as a co-polymer enhanced chitosan scaffolds bioactivity through the formation of an apatite layer

After 7 d of soaking in SBF solution, no CaP deposits could be detected on any of the scaffolds (results not shown). All spectra showed high peaks of carbon, which could be explained by chitosan (since it mainly consists of C, O and H) and the use of a carbon coating. Furthermore, traces of Ca, P, S, K, Mg were detected on the surface of all scaffolds, which could also be explained by the immersion in SBF.

After 21 d in SBF, CaP deposits could be observed on chitosan/gelatine blend scaffolds (CS-GEL-GPTMS and fCS-GEL-GPTMS) (Fig. 5a-d). The EDX spectra

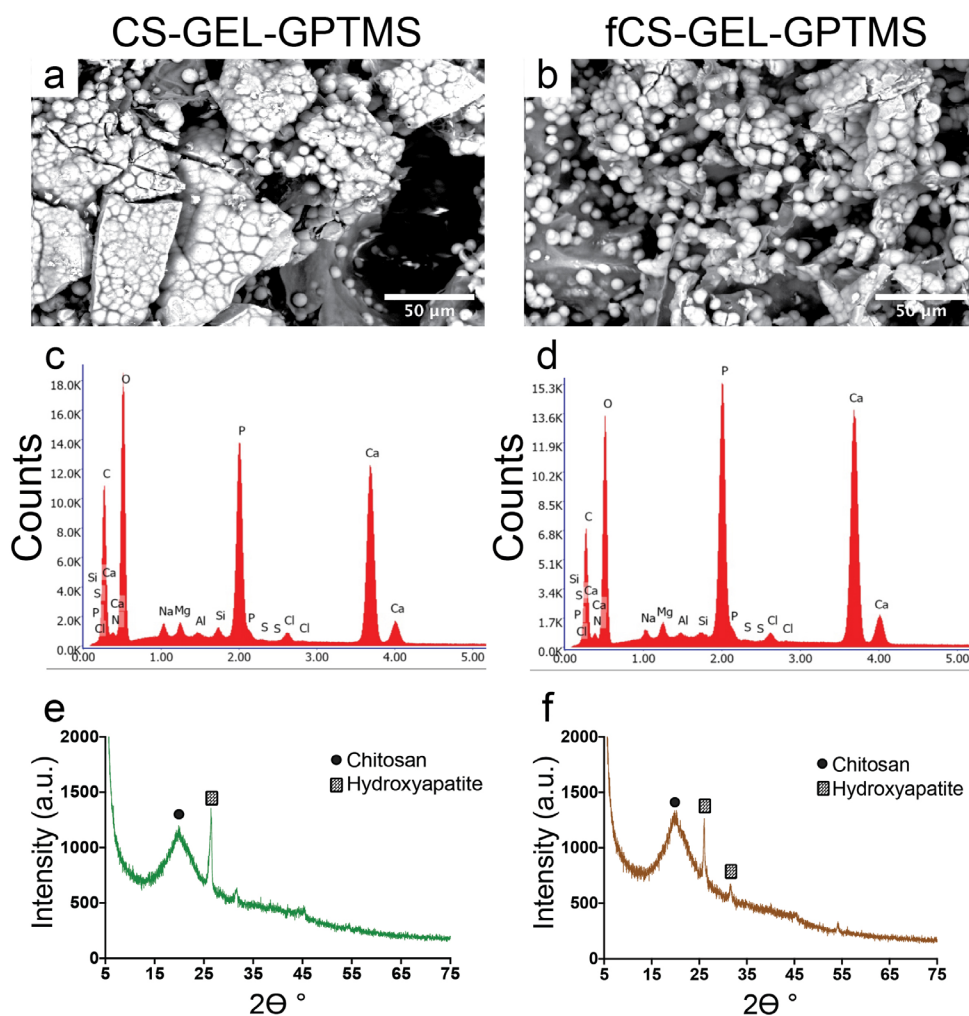


Fig. 5. Scaffold bioactivity. (a,b) Representative SEM images and (c,d) corresponding EDX point analysis after 21 d in SBF, showing high levels of Ca and P deposition characteristic of hydroxyapatite formation. (e,f) XRD analysis confirming the formation of hydroxyapatite crystals.

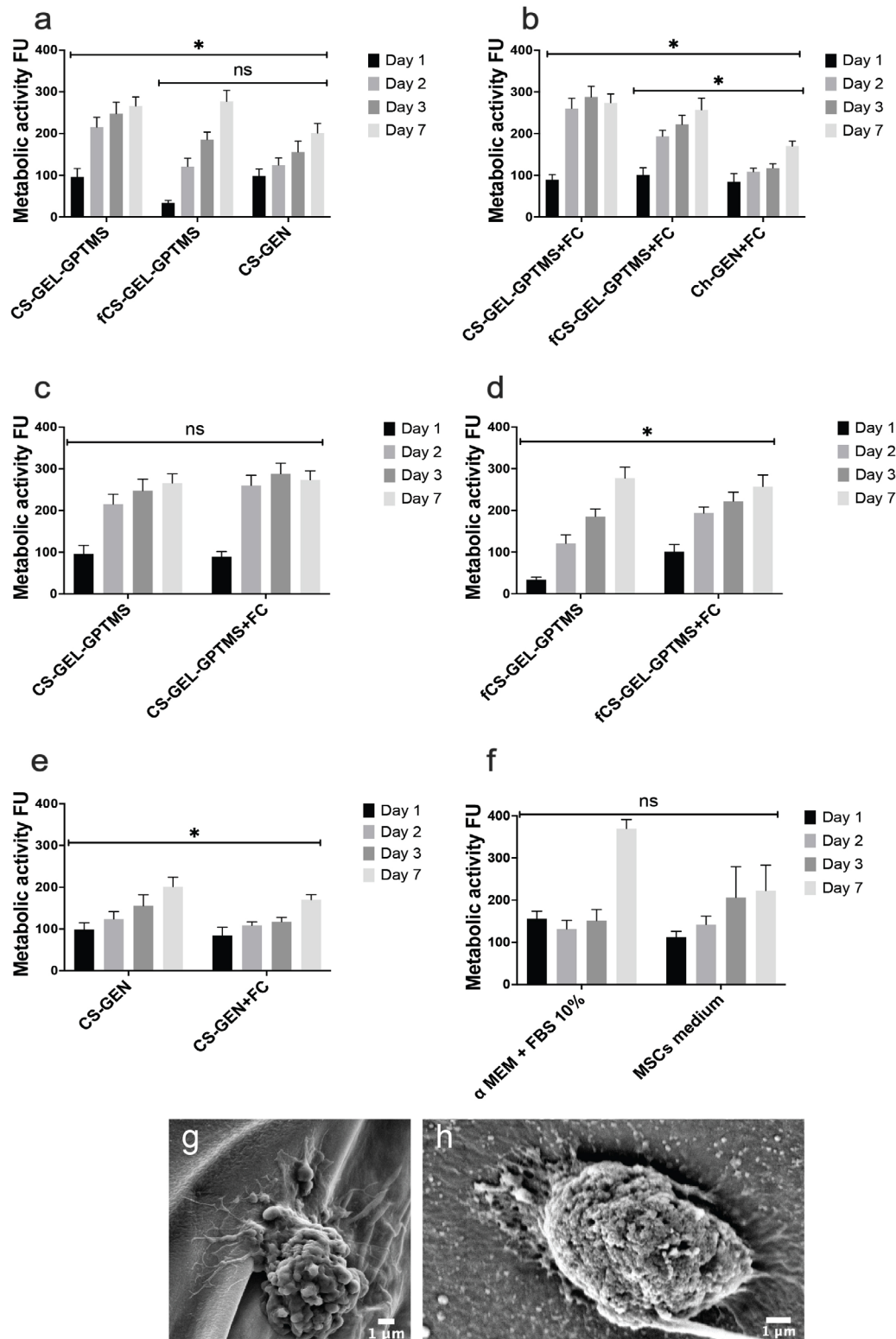


Fig. 6. hDPSCs metabolic activity. (a) hDPSCs metabolic activity up to 7 d in response to scaffolds showing a favourable cellular response to all chitosan scaffolds, with significantly higher viability in response to CS-GEL-GPTMS scaffolds over the experimental period. (b) Metabolic activity in response to scaffolds coated with fibronectin (FC). ANOVA showing significantly higher viability in response to CS-GEL-GPTMS with FC scaffolds compared to the other two groups and significantly higher viability for fCS-GEL-GPTMS with FC scaffolds compared to the Ch-GEN with FC scaffolds. (c) Cellular response to CS-GEL-GPTMS scaffolds was not affected by the addition of FC, while (d) a positive effect was observed with fCS-GEL-GPTMS and (e) a negative effect with CS-GEN scaffolds. (f) 2D controls in different cell culture media. (g,h) Representative SEM images for hDPSCs attached to the scaffold surface (g) CS-GEL-GPTMS and (h) fCS-GEL-GPTMS. Data are represented as mean \pm standard deviation. * statistically significant; ns: not significant. FU: fluorescence unit.

Table 1. Detected Ca (wt. %), P (wt. %) and Ca/P ratio of 5-point analysis on the animal- and fungal-derived chitosan/gelatine blend scaffolds (CS-GEL-GPTMS and fCS-GEL-GPTMS). Data are represented as mean \pm standard deviation.

Sample code	Ca (wt.%)	P (wt.%)	Ca/P ratio
CS-GEL-GPTMS	22.33 (\pm 9.55)	11.73 (\pm 5.55)	1.98 (\pm 0.22)
fCS-GEL-GPTMS	26.27 (\pm 3.62)	13.86 (\pm 1.65)	1.89 (\pm 0.07)

showed the presence of Si related to the use of GPTMS and C related to chitosan. Additionally, traces of SBF (Ca, P, S, K, Mg) and some NaCl crystals were detected at distinct positions on the surface of the scaffolds. However, the chitosan/gelatine blend scaffolds (CS-GEL-GPTMS and fCS-GEL-GPTMS) showed some clear Ca and P peaks (Fig. 5c,d). Moreover, the CaP deposits showed a typical cauliflower structure of hydroxyapatite crystals on the SEM images (Fig. 5a,b). XRD analysis at 21 d suggested the formation of HA crystals on the surface of chitosan/gelatine blend scaffolds (CS-GEL-GPTMS and fCS-GEL-GPTMS) (Fig. 5e,f). To further investigate the deposits on CS-GEL-GPTMS and fCS-GEL-GPTMS scaffolds, the average Ca/P ratio was calculated by examining 5 different points at the surface by EDX (Table 1). A Ca/P ratio of 1.98 and 1.89 was found for animal chitosan/gelatine blend scaffolds (CS-GEL-GPTMS) and fungal chitosan/gelatine blend scaffolds (fCS-GEL-GPTMS), respectively. It should be noted that small amounts of Ca and P were also detected on the CS-GEN scaffolds at very high magnification (results not shown). However, since this was only observed at a very small area on the scaffold surface, the Ca/P ratio was not further analysed.

Fabricated scaffolds supported hDPSCs attachment and viability

Overall, the 3 scaffold compositions tested all showed the ability to support hDPSCs attachment and viability as demonstrated by the increased metabolic activity over the experimental period, as assessed by alamarBlue assay (Fig. 6a-b). There was a significant ($p < 0.05$) effect on hDPSC metabolic activity based on scaffold composition [F (2, 128) = 32.81, $p < 0.0001$] and time point [F (3, 128) = 30.76, $p < 0.0001$]. *Post-hoc* comparisons by Tukey test showed a significantly higher metabolic activity in response to CS-GEL-GPTMS scaffolds when compared to the other 2 groups ($p < 0.05$), suggesting a better cell attachment and proliferation pattern (Fig. 6a). The addition of fibronectin did not affect cell behaviour in response to CS-GEL-GPTMS scaffolds ($p > 0.05$) (Fig. 6c). This was in contrast with the results obtained for fCS-GEL-GPTMS scaffolds, where a significant positive effect could be observed after the addition of fibronectin ($p < 0.05$) (Fig. 6d). Surprisingly, the addition of fibronectin had a slightly negative effect when added to the CS-GEN scaffolds as compared to scaffolds without fibronectin (Fig. 6e). There were no differences in cell metabolic activity in cells cultured as 2D controls in different culture media ($p > 0.05$)

(Fig. 6f), supporting the use of serum-free MSC medium in hDPSCs cultures.

Discussion

Dental conditions such as caries, trauma and developmental anomalies frequently affect the developing permanent teeth, leading to tissue or even whole tooth loss (Kassebaum *et al.*, 2014; Kassebaum *et al.*, 2017; Petti *et al.*, 2018). The roots of immature teeth with pulp necrosis fail to develop and are left functionally compromised on the long-term due to arrested dentine formation (Murray *et al.*, 2007). Dental tissue engineering has emerged as a valuable solution for dentine-pulp complex repair/regeneration and eventually tooth replacement through the fabrication of bioengineered tooth-root. Scaffolds are key elements in the development of any tissue engineering solution, as they provide a temporary 3D structures to support cellular attachment, migration, proliferation and guided differentiation (Ceccarelli *et al.*, 2017; Galler and D'Souza, 2011; Galler *et al.*, 2010). In general, scaffolds should possess the following characteristics: biocompatibility; inter-connected porosity; patient-specificity, with mechanical properties allowing surgical handling; biodegradability; and should mimic the ECM and promote appropriate cell behaviours (Albuquerque *et al.*, 2014; Huang and Garcia-Godoy, 2014; Larsson *et al.*, 2016). Chitosan is a natural biopolymer that possess several of the required scaffolds characteristics, as summarised in the introduction, in addition to antimicrobial properties and induction of M2 macrophage polarisation through elected immune-reaction profile (Caires *et al.*, 2018; 2016).

The present study focused on the fabrication and characterisation of customised scaffolds made of chitosan from different sources and cross-linkers for dental root tissue engineering. Chitosan scaffolds were prepared by means of emulsion freeze-drying using 3D-printed moulds. While moulds of basic geometries were applied, it can easily be appreciated how patient/tooth specific moulds and subsequently also scaffolds can be fabricated based on low-dose cone beam CT imaging (EzEldeen *et al.*, 2017) and inserted, for example, in the wide canals of immature teeth or bony defects for the delivery of bioactive molecules or stem cells.

Interconnected pores and appropriate pore diameter are required to promote cell seeding and

diffusion of cells, nutrients, oxygen, waste and growth factors (Hutmacher, 2001; Karageorgiou and Kaplan, 2005). The exact required porosity and pore diameter are dependent on the specific cell type, but it is hypothesised that the average pore diameter should be at least three times the cell size to ensure cell communication (Kim *et al.*, 2017). hDPSCs, which are targeted in dental tissue engineering, are about 10–15 μm in size, hence a minimal pore diameter of $\sim 45 \mu\text{m}$ is required. The porosity of the chitosan scaffolds fabricated in the present study ranged between 40 and 112 μm , depending on the chitosan source and the addition of gelatine as a co-polymer (Fig. 2a–g), which should be sufficient for hDPSC attachment and proliferation. Moreover, as a result of the directional freezing applied during emulsion freeze-drying, pores were radially oriented, as shown by the structural characterisation using SEM and nano-CT (Fig. 2). This directionality mimicked the architecture of natural dentine (Bertassoni, 2017) and might be favourable for hDPSC attachment, proliferation, guided differentiation into odontoblasts and subsequent dentine deposition. Therefore, future studies should focus on determining the effect of different pore diameters and 3D architecture on dental stem cells behaviour.

To improve the stability of the chitosan scaffolds, gelatine was added as a co-polymer and different cross-linking agents were applied (GPTMS or genipin). FTIR analysis proved the successful cross-linking of chitosan and chitosan-gelatine by both GPTMS and genipin (Fig. 3a–c). Moreover, animal and fungal chitosan showed similar chemical composition and cross-linking behaviour. This successful co-polymerisation with gelatine increased the compressive strength of the scaffolds (CS-GEL-GPTMS and fCS-GEL-GPTMS) compared to CS-GEN, suggesting improved handling properties. In addition, chitosan source influenced the compressive strength since scaffolds from animal chitosan had a compression modulus 3-fold higher than fungal chitosan. Very limited information can be found in the literature on the application of fungal chitosan in tissue engineering. However, Nwe *et al.* (2009) reported a 1.5-fold higher tensile strength for scaffolds from fungal chitosan (*Gongronella butleri*) (MW = 50 kDa) when compared to scaffolds from animal chitosan. The fungal chitosan used in the present study was obtained from *Aspergillus niger* (MW < 30 kDa), suggesting that fungal species and MW would influence the properties of fungal chitosan scaffolds.

Another significant effect of the chitosan source was the degradation rate. Scaffolds from fungal chitosan (fCS-GEL-GPTMS) lost 80 % of their weight by 21 d when compared to 40 % for scaffolds from animal chitosan (CS-GEL-GPTMS) (Fig. 4a). This could be due to a lower MW and DA. This faster degradation rate for fungal chitosan was also reported by Nwe *et al.* (2009) to be 11 % at 14 d, compared to 2–5 % for scaffolds from animal sources. It can be

hypothesised that this faster degradation rate would be beneficial for endodontic applications, where the scaffold is protected by the root canal walls and is expected to degrade at a slower rate. Furthermore, the type of crosslinker seems to influence the degradation rate, suggesting that the use of genipin (CS-GEN) led to a faster degradation compared to GPTMS (CS-GEL-GPTMS), possibly related to its larger pore diameter or the natural origin of genipin.

The formation of calcium phosphates, especially hydroxyapatite [$(\text{Ca}_{10}(\text{PO}_4)_6(\text{OH})_2)$], having a similar chemical composition to that of the mineral phase of bone and dentine, is important for mimicking the mineralised tissue of natural dentine or alveolar bone (Lluch *et al.*, 2009; Manjubala *et al.*, 2006). The capability of the chitosan scaffolds to stimulate the formation of an apatite layer *in vitro* was tested by immersing the scaffolds in SBF for 7 and 21 d. The results of the EDX analysis showed clear Ca and P peaks that were confirmed by XRD to be hydroxyapatite crystals for CS-GEL-GPTMS and fCS-GEL-GPTMS scaffolds (Fig. 5a–f). Moreover, Ca/P ratios of 1.98 and 1.89 were found for CS-GEL-GPTMS and fCS-GEL-GPTMS scaffolds, respectively (Table 1). Those values are close to the Ca/P ratio of mineral phase of human, which is 1.67. This is an important parameter, as it has been hypothesised that it is easier for DPSCs to attach and proliferate on a substrate with a ratio close to the one of natural ECM (Liao and Ho, 2010). Other studies have shown that a ratio of approximately 1.85 is characteristic of non-stoichiometric hydroxyapatite phase (Chatzistavrou *et al.*, 2015). Overall, the bioactivity testing results indicated that the combination of gelatine as a co-polymer and cross-linking using GPTMS could have a positive effect on the formation of an apatite layer on the surface of the chitosan scaffolds. Therefore, these chitosan scaffolds (CS-GEL-GPTMS and fCS-GEL-GPTMS) are suitable for the regeneration of mineralised tissues such as dentine or alveolar bone.

Several authors have successfully reported on the application of different hydrogels in dental pulp tissue engineering (Dissanayaka *et al.*, 2015; Galler *et al.*, 2018; Hilkens *et al.*, 2017; Nakashima *et al.*, 2017). From those hydrogels, fibrin seems to be an excellent candidate for pulp tissue engineering (Galler *et al.*, 2018). Moreover, it has been demonstrated that chitosan incorporation in fibrin hydrogels could enhance the antibacterial properties and immunomodulation in a dental pulp regeneration context (Ducret *et al.*, 2019; Renard *et al.*, 2020). Therefore, gaining a deeper understanding on the effect of chitosan from different sources and the use of different cross-linkers on scaffold properties could aid in the optimisation of such hydrogel systems.

hDPSCs, SCAPs or SHED are mesenchymal stem/stromal cells that pose the potential to differentiate into numerous cell types *in vitro* including, odontoblasts, osteoblasts, chondroblasts, adipocytes and neuronal cells (Bronckaers *et al.*, 2013; Bronckaers *et al.*, 2014; Ratajczak *et al.*, 2016). The relative ease of

accessibility from teeth (*e.g.* from extracted wisdom molars or exfoliated primary teeth) (Hilkens *et al.*, 2016) renders them a valuable tool for studying and exploring tissue regeneration possibilities in the dentoalveolar and craniofacial regions. hDPSCs were used in the present study to evaluate the scaffolds' biocompatibility. hDPSCs were seeded and cultured in serum-free MSC medium to avoid false positive cell attachment results due to the presence of FBS in commonly used cell culture mediums for hDPSCs. Results demonstrated the suitability of serum-free MSC medium for maintenance and proliferation of hDPSCs (Fig. 6f). This is an important parameter for future translational clinical research to avoid the use of animal components in human cell cultures. The cell metabolic activity delivers indirect information on viability and attachment to porous scaffolds surface (Zhou *et al.*, 2013). All scaffold compositions supported cell viability and attachment up to 7 d (Fig. 6a,b), however CS-GEL-GPTMS group had the best performance, followed by fCS-GEL-GPTMS (Fig. 6a). This could be explained by the presence of the integrin-binding RGD-like sequence in gelatine, which will promote cellular attachment (Kumar *et al.*, 2017). Moreover, it has been reported that the Si-OH and Si-O-Si groups, derived from GPTMS, can promote MG-63 osteoblast-like cells attachment and proliferation, indicating the importance of silicate ions in the promotion of cell differentiation (Tondaturo *et al.*, 2011). These Si-OH and Si-O-Si groups were also observed in the FTIR data from the current study, which may offer an additional explanation for the hDPSC favourable response to CS-GEL-GPTMS and fCS-GEL-GPTMS groups. Moreover, hDPSC attachment and proliferation seemed to be inversely proportional to the pore diameter as CS-GEN scaffolds had the largest pore diameter, followed by fCS-GEL-GPTMS and CS-GEL-GPTMS (Fig. 2g and 6a,b). Future studies should apply deep learning algorithms (*in silico* modelling) on combined structural and biological data to identify the main variables influencing specific cellular responses for optimised scaffold design and fabrication (Geris *et al.*, 2018).

Conclusion

The present study presented data on a practical fabrication method of scaffolds with organised porosity, utilising CAD and 3D printing, which have become a common clinical practice in the last decade. The use of fungal-derived chitosan was explored for its desirable properties of reduced risk of allergic reaction, low molecular weight and enhanced antimicrobial properties. This was followed by a comprehensive characterisation showing the effect of chitosan source, co-polymerisation with gelatine and different cross-linkers on the structural and biological properties of the scaffolds. The proposed scaffolds combined with bioactive molecules could have a

direct clinical application in cell-free regenerative endodontics of immature teeth to control infections, induce dentine formation and root development. Moreover, tailored scaffolds could be modified through the addition of inorganic components such as tricalcium phosphate or bioactive glass for alveolar bone regeneration. Further work will focus on obtaining a deeper understanding of stem-cell and immune-cell behaviour in response to the scaffolds to optimise their application in dento-alveolar tissue engineering.

Acknowledgements

The study was supported by the Research Council of KU Leuven, grant number C24/18/068. AB acknowledges the receipt of a starting grant from Internal Funds KU Leuven (STG/17/024). The authors would like to thank Prof. Koen Binnemans (KU Leuven, Department of Chemistry) for the use of the FTIR device. Also thanks to Prof. Ivo Lambrichts (U Hasselt) and Prof. Annelies Bronckaers (U Hasselt) for providing the hDPSCs and the continued collaboration.

ME, JL, AB and RJ contributed to the conception, design, data acquisition, analysis, interpretation as well as drafted and critically revised the manuscript; ZN, DM and MC contributed to data acquisition, analysis, interpretation and critically revised the manuscript. All authors gave final approval and agreed to be accountable for all aspects of the study. The authors deny any conflicts of interest.

References

- Albuquerque MT, Valera MC, Nakashima M, Nor JE, Bottino MC (2014) Tissue-engineering-based strategies for regenerative endodontics. *J Dent Res* **93**: 1222-1231.
- Amancio MA, Pinto EP, Matos RS, Nobre FX, Brito WR, da Fonseca Filho HD (2020) Nanoscale morphology and fractal analysis of TiO₂ coatings on ITO substrate by electrodeposition. *J Microsc.* DOI: 10.1111/jmi.12990.
- Austah O, Joon R, Fath WM, Chrepa V, Diogenes A, EzEldeen M, Couve E, Ruparel NB (2018) Comprehensive characterization of 2 immature teeth treated with regenerative endodontic procedures. *J Endod* **44**: 1802-1811.
- Batista ACdL, Souza Neto FEd, Paiva WdS (2018) Review of fungal chitosan: past, present and perspectives in Brazil. *Polímeros* **28**: 275-283.
- Bertassoni LE (2017) Dentin on the nanoscale: hierarchical organization, mechanical behavior and bioinspired engineering. *Dent Mater* **33**: 637-649.
- Bronckaers A, Hilkens P, Fanton Y, Struys T, Gervois P, Politis C, Martens W, Lambrichts I (2013) Angiogenic properties of human dental pulp stem

cells. *PLoS One* **8**: e71104. DOI: 10.1371/journal.pone.0071104.

Bronckaers A, Hilkens P, Martens W, Gervois P, Ratajczak J, Struys T, Lambrechts I (2014) Mesenchymal stem/stromal cells as a pharmacological and therapeutic approach to accelerate angiogenesis. *Pharmacol Ther* **143**: 181-196.

Caires HR, Barros da Silva P, Barbosa MA, Almeida CR (2018) A co-culture system with three different primary human cell populations reveals that biomaterials and MSC modulate macrophage-driven fibroblast recruitment. *J Tissue Eng Regen Med* **12**: e1433-e1440.

Caires HR, Esteves T, Quelhas P, Barbosa MA, Navarro M, Almeida CR (2016) Macrophage interactions with polylactic acid and chitosan scaffolds lead to improved recruitment of human mesenchymal stem/stromal cells: a comprehensive study with different immune cells. *J R Soc Interface* **3**: 20160570. DOI: 10.1098/rsif.2016.0570.

Ceccarelli G, Presta R, Benedetti L, Cusella De Angelis MG, Lupi SM, Rodriguez YBR (2017) Emerging perspectives in scaffold for tissue engineering in oral surgery. *Stem Cells Int* **2017**: 4585401. DOI: 10.1155/2017/4585401.

Chao A-C (2008) Preparation of porous chitosan/GPTMS hybrid membrane and its application in affinity sorption for tyrosinase purification with *Agaricus bisporus*. *J Membr Sci* **311**: 306-318.

Chatzistavrou X, Velamakanni S, DiRenzo K, Lefkelidou A, Fenno JC, Kasuga T, Boccaccini AR, Papagerakis P (2015) Designing dental composites with bioactive and bactericidal properties. *Mater Sci Eng C Mater Biol Appl* **52**: 267-272.

Chen J, Que W, Xing Y, Lei B (2015) Fabrication of biomimetic polysiloxane-bioactive glass-chitosan hybrid monoliths with high apatite-forming bioactivity. *Ceram Int* **41**: S393-S398.

Chiono V, Pulieri E, Vozzi G, Ciardelli G, Ahluwalia A, Giusti P (2008) Genipin-crosslinked chitosan/gelatin blends for biomedical applications. *J Mater Sci Mater Med* **19**: 889-898.

Connell LS, Romer F, Suarez M, Valliant EM, Zhang Z, Lee PD, Smith ME, Hanna JV, Jones JR (2014) Chemical characterisation and fabrication of chitosan-silica hybrid scaffolds with 3-glycidoxypopyl trimethoxysilane. *J Mater Chem B* **2**: 668-680.

Cui L, Jia J, Guo Y, Liu Y, Zhu P (2014) Preparation and characterization of IPN hydrogels composed of chitosan and gelatin cross-linked by genipin. *Carbohydr Polym* **99**: 31-38.

Dimida S, Barca A, Cancelli N, De Benedictis V, Raucci MG, Demitri C (2017) Effects of genipin concentration on cross-linked chitosan scaffolds for bone tissue engineering: structural characterization and evidence of biocompatibility features. *Int J Polym Sci* **2017**: 1-8.

Dissanayaka WL, Hargreaves KM, Jin L, Samaranyake LP, Zhang C (2015) The interplay of dental pulp stem cells and endothelial cells in an

injectable peptide hydrogel on angiogenesis and pulp regeneration *in vivo*. *Tissue Eng Part A* **21**: 550-563.

Ducret M, Montebault A, Josse J, Padeloup M, Celle A, Benchrih R, Mallein-Gerin F, Alliot-Licht B, David L, Farges JC (2019) Design and characterization of a chitosan-enriched fibrin hydrogel for human dental pulp regeneration. *Dent Mater* **35**: 523-533.

EzEldeen M, Stratis A, Coucke W, Codari M, Politis C, Jacobs R (2017) As low dose as sufficient quality: optimization of cone-beam computed tomographic scanning protocol for tooth autotransplantation planning and follow-up in children. *J Endod* **43**: 210-217.

EzEldeen M, Van Gorp G, Van Dessel J, Vandermeulen D, Jacobs R (2015) 3-dimensional analysis of regenerative endodontic treatment outcome. *J Endod* **41**: 317-324.

Fakhri E, Eslami H, Maroufi P, Pakdel F, Taghizadeh S, Ganbarov K, Yousefi M, Tanomand A, Yousefi B, Mahmoudi S, Kafil HS (2020) Chitosan biomaterials application in dentistry. *Int J Biol Macromol* **162**: 956-974.

Galler KM, Brandl FP, Kirchhof S, Widbillier M, Eidt A, Buchalla W, Gopferich A, Schmalz G (2018) Suitability of different natural and synthetic biomaterials for dental pulp tissue engineering. *Tissue Eng Part A* **24**: 234-244.

Galler KM, D'Souza RN (2011) Tissue engineering approaches for regenerative dentistry. *Regen Med* **6**: 111-124.

Galler KM, D'Souza RN, Hartgerink JD (2010) Biomaterials and their potential applications for dental tissue engineering. *J Mater Chem* **20**: 8730-8746.

Gao L, Gan H, Meng Z, Gu R, Wu Z, Zhang L, Zhu X, Sun W, Li J, Zheng Y, Dou G (2014) Effects of genipin cross-linking of chitosan hydrogels on cellular adhesion and viability. *Colloids Surf B Biointerfaces* **117**: 398-405.

Gathani KM, Raghavendra SS (2016) Scaffolds in regenerative endodontics: a review. *Dent Res J (Isfahan)* **13**: 379-386.

Geris L, Lambrechts T, Carlier A, Papantoniou I (2018) The future is digital: *in silico* tissue engineering. *Curr Opin Biomed Eng* **6**: 92-98.

Hamedi H, Moradi S, Hudson SM, Tonelli AE (2018) Chitosan based hydrogels and their applications for drug delivery in wound dressings: a review. *Carbohydr Polym* **199**: 445-460.

Hilkens P, Bronckaers A, Ratajczak J, Gervois P, Wolfs E, Lambrechts I (2017) The angiogenic potential of dpsc and scaps in an *in vivo* model of dental pulp regeneration. *Stem Cells Int* **2017**: 2582080. DOI: 10.1155/2017/2582080.

Hilkens P, Driesen RB, Wolfs E, Gervois P, Vanganswinkel T, Ratajczak J, Dillen Y, Bronckaers A, Lambrechts I (2016) Cryopreservation and banking of dental stem cells. *Adv Exp Med Biol* **951**: 199-235.

Hilkens P, Gervois P, Fanton Y, Vanormelingen J, Martens W, Struys T, Politis C, Lambrechts I, Bronckaers A (2013) Effect of isolation methodology on

stem cell properties and multilineage differentiation potential of human dental pulp stem cells. *Cell Tissue Res* **353**: 65-78.

Huang GT, Garcia-Godoy F (2014) Missing concepts in *de novo* pulp regeneration. *J Dent Res* **93**: 717-724.

Hutmacher DW (2001) Scaffold design and fabrication technologies for engineering tissues—state of the art and future perspectives. *J Biomater Sci Polym Ed* **12**: 107-124.

Karageorgiou V, Kaplan D (2005) Porosity of 3D biomaterial scaffolds and osteogenesis. *Biomaterials* **26**: 5474-5491.

Kassebaum NJ, Bernabe E, Dahiya M, Bhandari B, Murray CJ, Marcenes W (2014) Global burden of severe periodontitis in 1990-2010: a systematic review and meta-regression. *J Dent Res* **93**: 1045-1053.

Kassebaum NJ, Smith AGC, Bernabe E, Fleming TD, Reynolds AE, Vos T, Murray CJL, Marcenes W, Collaborators GBDOH (2017) Global, Regional, and national prevalence, incidence, and disability-adjusted life years for oral conditions for 195 countries, 1990-2015: a systematic analysis for the Global Burden of Diseases, Injuries, and Risk Factors. *J Dent Res* **96**: 380-387.

Kim HY, Kim HN, Lee SJ, Song JE, Kwon SY, Chung JW, Lee D, Khang G (2017) Effect of pore sizes of PLGA scaffolds on mechanical properties and cell behaviour for nucleus pulposus regeneration *in vivo*. *J Tissue Eng Regen Med* **11**: 44-57.

Klein MP, Hackenhaar CR, Lorenzoni ASG, Rodrigues RC, Costa TMH, Ninow JL, Hertz PF (2016) Chitosan crosslinked with genipin as support matrix for application in food process: support characterization and beta-D-galactosidase immobilization. *Carbohydr Polym* **137**: 184-190.

Kokubo T, Takadama H (2006) How useful is SBF in predicting *in vivo* bone bioactivity? *Biomaterials* **27**: 2907-2915.

Kumar P, Dehiya BS, Sindhu A (2017) Comparative study of chitosan and chitosan–gelatin scaffold for tissue engineering. *Int Nano Lett* **7**: 285-290.

Kwon YS, Lim ES, Kim HM, Hwang YC, Lee KW, Min KS (2015) Genipin, a cross-linking agent, promotes odontogenic differentiation of human dental pulp cells. *J Endod* **41**: 501-507.

Larsson L, Decker AM, Nibali L, Pilipchuk SP, Berglundh T, Giannobile WV (2016) Regenerative medicine for periodontal and peri-implant diseases. *J Dent Res* **95**: 255-266.

Liao CT, Ho MH (2010) The fabrication of biomimetic chitosan scaffolds by using SBF treatment with different crosslinking agents. *Membranes (Basel)* **1**: 3-12.

Liu L, Gao Q, Lu X, Zhou H (2016) *In situ* forming hydrogels based on chitosan for drug delivery and tissue regeneration. *Asian J Pharm Sci* **11**: 673-683.

Liu Y-L, Su Y-H, Lai J-Y (2004) *In situ* crosslinking of chitosan and formation of chitosan–silica hybrid membranes with using γ -glycidoxypolytrimetho-

xysilane as a crosslinking agent. *Polymer* **45**: 6831-6837.

Lluch AV, Fernandez AC, Ferrer GG, Pradas MM (2009) Bioactive scaffolds mimicking natural dentin structure. *J Biomed Mater Res B Appl Biomater* **90**: 182-194.

Manjubala I, Scheler S, Bossert J, Jandt KD (2006) Mineralisation of chitosan scaffolds with nano-apatite formation by double diffusion technique. *Acta Biomater* **2**: 75-84.

Meschi N, EzEldeen M, Torres Garcia AE, Jacobs R, Lambrechts P (2018) A retrospective case series in regenerative endodontics: trend analysis based on clinical evaluation and 2- and 3-dimensional radiology. *J Endod* **44**: 1517-1525.

Meschi N, Hilkens P, Van Gorp G, Strijbos O, Mavridou A, Cadenas de Llano Perula M, Lambrichts I, Verbeken E, Lambrechts P (2019) Regenerative endodontic procedures posttrauma: immunohistologic analysis of a retrospective series of failed cases. *J Endod* **45**: 427-434.

Mi F-L, Shyu S-S, Peng C-K (2005) Characterization of ring-opening polymerization of genipin and pH-dependent cross-linking reactions between chitosan and genipin. *J Polymer Science Part A: Polymer Chemistry* **43**: 1985-2000.

Militký J, Bajzík V (2001) Surface roughness and fractal dimension. *J Textile Institute* **92**: 91-113.

Murray PE, Garcia-Godoy F, Hargreaves KM (2007) Regenerative endodontics: a review of current status and a call for action. *J Endod* **33**: 377-390.

Nakashima M, Iohara K, Murakami M, Nakamura H, Sato Y, Arijii Y, Matsushita K (2017) Pulp regeneration by transplantation of dental pulp stem cells in pulpitis: a pilot clinical study. *Stem Cell Res Ther* **8**: 61. DOI: 10.1186/s13287-017-0506-5.

Nwe N, Furuike T, Tamura H (2009) The mechanical and biological properties of chitosan scaffolds for tissue regeneration templates are significantly enhanced by chitosan from *Gongronella butleri*. *Materials* **2**: 374-398.

Petti S, Glendor U, Andersson L (2018) World traumatic dental injury prevalence and incidence, a meta-analysis—one billion living people have had traumatic dental injuries. *Dent Traumatol* **34**: 71-86.

Ratajczak J, Hilkens P, Gervois P, Wolfs E, Jacobs R, Lambrichts I, Bronckaers A (2016) Angiogenic capacity of periodontal ligament stem cells pretreated with deferroxamine and/or fibroblast growth factor-2. *PLoS One* **11**: e0167807. DOI: 10.1371/journal.pone.0167807.

Renard E, Amiaud J, Delbos L, Charrier C, Montebault A, Ducret M, Farges JC, David L, Alliot-Licht B, Gaudin A (2020) Dental pulp inflammatory/immune response to a chitosan-enriched fibrin hydrogel in the pulpotomised rat incisor. *Eur Cell Mater* **40**: 74-87.

Sakai S, Kawakami K (2007) Synthesis and characterization of both ionically and enzymatically cross-linkable alginate. *Acta Biomater* **3**: 495-501.

Šapić IM, Bistričić L, Volovšek V, Dananić V (2014) Vibrational analysis of 3-glycidoxypropyltrimethoxysilane polymer. *Macromol Symp* **339**: 122-129.

Schindelin J, Arganda-Carreras I, Frise E, Kaynig V, Longair M, Pietzsch T, Preibisch S, Rueden C, Saalfeld S, Schmid B, Tinevez JY, White DJ, Hartenstein V, Eliceiri K, Tomancak P, Cardona A (2012) Fiji: an open-source platform for biological-image analysis. *Nat Methods* **9**: 676-682.

Sharma S, Srivastava D, Grover S, Sharma V (2014) Biomaterials in tooth tissue engineering: a review. *J Clin Diagn Res* **8**: 309-315.

Tonda-Turo C, Gentile P, Saracino S, Chiono V, Nandagiri VK, Muzio G, Canuto RA, Ciardelli G (2011) Comparative analysis of gelatin scaffolds

crosslinked by genipin and silane coupling agent. *Int J Biol Macromol* **49**: 700-706.

Zhou X, Holsbeeks I, Impens S, Sonnaert M, Bloemen V, Luyten F, Schrooten J (2013) Noninvasive real-time monitoring by alamarBlue((R)) during *in vitro* culture of three-dimensional tissue-engineered bone constructs. *Tissue Eng Part C Methods* **19**: 720-729.

Editor's note: There were no questions from reviewers for this paper, therefore there is no Discussion with Reviewers section.

The Scientific Editor responsible for this paper was Thimios Mitsiadis.